sciendo

POLISH MARITIME RESEARCH 4 (112) 2021 Vol. 28; pp. 20-29
10.2478/pomr-2021-0046

WIND TUNNEL EXPERIMENT OF MULTI-MODE ARC SAIL DEVICE

Huawu Zhang*[1]
Yihuai Hu[1]
Jianhai He[2]
[1] Shanghai Maritime University, China
[2] Shanghai University of Engineering Science, China

* Corresponding author: *zhanghw@shmtu.edu.cn (H. Zhang)*

ABSTRACT

A ship's wind energy utilization device with multi-mode arc-shaped sails is designed, which have different working modes for sail-assisting or wind power generation according to the ship's navigation. The structural characteristics and working principles of this device are firstly described in this paper. Three sets of arc-shaped sails with different thickness (4.5 cm, 11.3 cm, 21.7 cm) were designed. Wind tunnel experiments were carried out in the respects of sail-assisting performance and wind-power generation to determine the best sail blade shape and to verify the energy-saving effect of this device. Experiments show that the sail with the smallest thickness (4.5 cm) has a better boosting effect than others, and the sail with the largest thickness (21.7 cm) has the best wind power generation performance. Considering the lateral force and the structural strength of the support, in the case of the comprehensive evaluation for the boosting and power generation performance, it is considered that the intermediate thickness (11.3 cm) is the best choice. The device has a good comprehensive energy utilization effect and has development and application value.

Keywords: marine engineering, multi-mode arc sail device, wind tunnel test, sail-assisted navigation, wind power generation

INTRODUCTION

Nowadays, shipping industries have become big energy consumers and the main source of air pollutants such as NO_X, SO_X, and particulate matter (PM). It was estimated that the overall amount of harmful gas emission from ships is three times that of on-shore enterprises and land transportation. Environmental protection regulations are becoming better and stricter. The Marine Environment Protection Committee (MEPC) of the International Maritime Organization (IMO) has issued a series of resolutions and mandatory requirements to control greenhouse gas (GHG) and harmful gas emissions from global ships [1, 2], which brings great pressure to shipping enterprises. Adjusting the energy structure, reducing energy consumption, reducing harmful gases and greenhouse gas emissions, and enhancing energy security has become the focus of international attention. How to take effective energy-saving measures has become one of the great concern issues of shipping enterprises.

Wind energy is a clean, safe, and renewable energy that is widely distributed and inexhaustible. The use of wind energy has no pollution to the environment, no ecologic damage, and has good environmental and ecological benefits. It is of great significance to the sustainable development for human society and shipping industries.

The main ways to harness wind energy onboard ships are sail-assisted navigation and wind power generation [3, 4]. Sails have a long history as the power source of ships. Sailing devices can only be used as sail aids when the ship is sailing. Some ships, such as yachts, fishing boats, and engineering ships do not have a long sail duration. They are often moored in berths or on the water for recreational or productive purposes and are unable to utilize wind energy. However, the ship's wind power generation devices are only used to generate electricity and cannot be used for sail-assistance.

Fu Yu [5] from Wuhan University of Technology designed a dual-purpose wind energy utilization device for sail-assisted navigation and wind power generation according to the route

characteristics of river-sea direct bulk carriers. He carried out simulation calculations and economic analysis on the device, but prototype tests and shipboard tests of the device were not available. The ship's wind energy utilization mode is single and cannot be flexibly adjusted according to the actual situation of the ship's navigation. This causes the ship to be inefficient in the utilization of wind energy during the whole operation cycle. It also lacks a simple and effective wind energy utilization device that can realize both wind-assisted navigation and wind power generation.

A multi-mode ship wind utilization device based on arc-shaped sails was proposed, which can adopt different modes under different conditions to combine the conversion of two working modes and improve the utilization efficiency of wind power. When the ship encounters favorable wind direction, the fuel consumption of the ship is reduced with the assistance by the wind. When the ship is docked or anchored, wind power generation can be carried out, which will greatly improve the comprehensive utilization efficiency of wind energy, especially suitable for engineering operation ships, fishing ships, and yachts with variable sailing conditions. To solve the optimal aerodynamic optimization design of the sail sheet, force, and power generation tests were conducted using a wind tunnel laboratory to verify the energy-saving performance of the device and provide a basis for the practical ship application of the multi-mode arc sail device.

MULTI-MODE SHIP WIND ENERGY UTILIZATION DEVICE

The overall structure of the device is shown in Fig. 1. It is supported by the main column, a beam, and a mast that carries two arc-shaped sail blades with the beam being connected to the main column. Three sets of electromagnets are symmetrically arranged on the main column, and the removable connecting rods are controlled to insert and withdraw the three fixed holes on the outer edge of the sail blade to form a blade locking mechanism. A disc generator is connected to the lower part of the column, which rotates and generates electricity. A stepper motor is mounted by its side on a movable tray. It can be separated from the main column when the wind power is generated and can be moved to the upright position when the sail assists the navigation and meshed with gears to change the sail angle according to different wind directions for providing maximum boosting force to the ship.

When the device is converted to the sail-assisted mode, the windward sides of both blades are in the same direction and locked, as shown in Fig. 1. The stepper motor is engaged with the main column through a conical snap ring to rotate the main column and adjust the sail angle for wind-assisted sailing. When the device needs to switch to power generation mode, moving the tray separates the gear of the stepper motor from the gear on the column. At the same time, one side of the sail blade rotates 180 degrees, reversing the sail on the other side. The position of the blade is shown in Fig. 13, forming a resistant-type wind turbine with power being generated by the disc motor connected to the column.

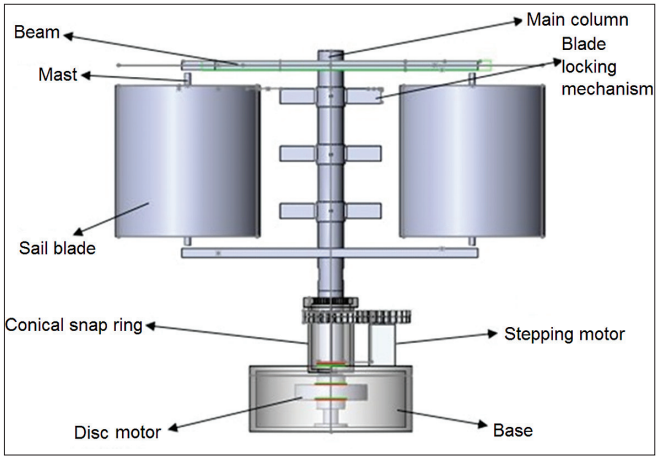

Fig. 1. Structure of multi-mode arc sail device

TEST EQUIPMENT AND TEST DEVICE MODEL

WIND TUNNEL

The wind tunnel used in the test is a closed-loop wind tunnel in the wind tunnel laboratory. The rated power is 132 kW and the frequency conversion motor drives the operation. The wind speed is controlled by a closed-loop. The test wind speed can be conveniently and accurately controlled continuously between 1–40 m/s. Airflow stability ≤ ± 0.365%, airflow turbulence ≤ 0.275%, and airflow unevenness ≤ ± 0.28%.

The test turntable is equipped in the test section of the wind tunnel. The rotation angle of the turntable is adjusted by a servo motor from -10° to 370° precisely and can be as accurate as 0.1° to change the deflection angle between the incoming flow and the sail model.

AERODYNAMIC MEASUREMENT SYSTEM

The six-component force measuring balance mounted on the turntable is used to measure the forces of the sail. The test wind speed is measured by a pitot tube and fed back to the control system to achieve wind speed via closed-loop control. The data of the six channels measured by the balance are collected by two sampling plates and output by the data processing computer. The forces and torques in three directions can be obtained directly.

The test model is connected to the measuring balance through the base. The test model and the measuring balance rotate with the turntable together to change the sail's different angles of attack. The force measurement in the test is based on the balance coordinate system. Since the balance is rotated by the turntable, the forces measured require a coordinate transformation. The zero position is the initial position, and the balance coordinate axis system is aligned with the wind tunnel coordinate axis system.

In this test, according to the mounting position of the model, the forces in the vertical direction can be ignored, and the F_X and F_Z values in the horizontal plane of the balance can be recorded during the test. This force diagram is shown in Fig. 4.

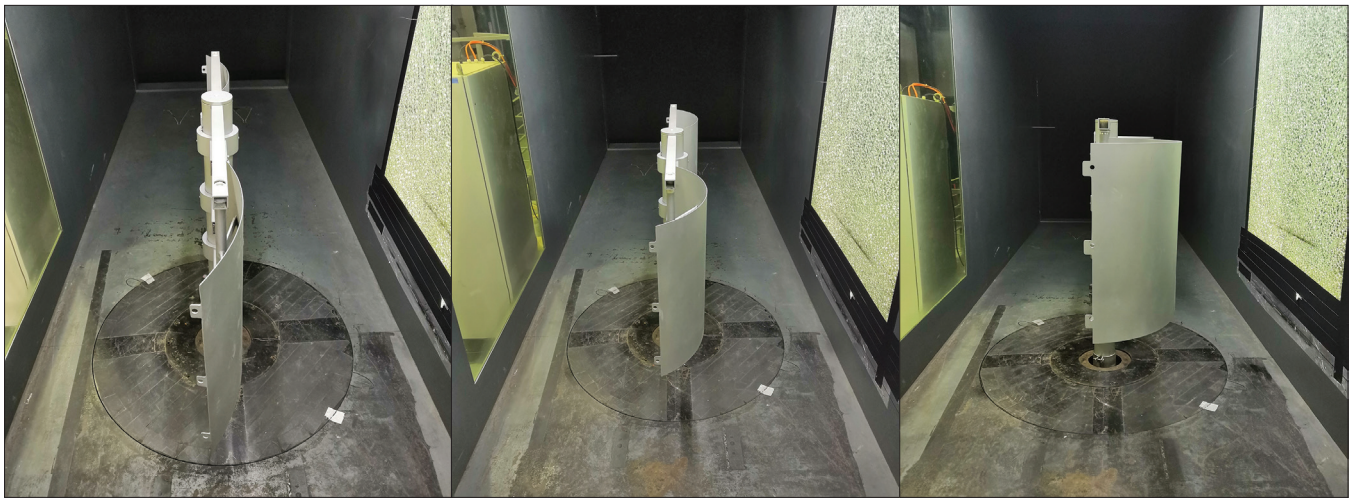

Fig. 2. Installation's diagram of a multi-mode sailing device in the wind tunnel

TEST DEVICE

In this experiment, three groups of sail blades with different curvatures (thickness) were designed for comparison. In order to study the effect of different sail thicknesses (different camber ratios) on sail boosting and power generation, several sets of sails with different thicknesses were designed and corresponded to represent a certain range of camber ratios values. According to Z. Xiangming [6], the boosting characteristics of arc sails with different camber ratios in the range of 0.1–0.14 were studied. Their findings showed that the camber ratio of 0.14 has better aerodynamic performance. Combining the actual need of this study to consider both boosting and power generation modes, the two sail types with camber ratios in the range of 0.25 and one sail type exceeding the range of 0.25 camber ratios were designed as representatives for this study. From the perspective of refinement and optimization, more sails with different camber ratios need to be designed, but this study is mainly to give the combined effect of boosting and power generation on the new device as a whole, so an arc-shaped sail with the parameters shown in Table 1 was chosen. According to the increasing direction of sail thickness, they were numbered as No. 1, No. 2, and No. 3 in sequence. The installations of the test setup are shown in Fig. 2, with the specific dimensions are shown in Table 1 and Fig. 3.

Tab. 1. Basic parameters of sail blades

NO.	Windward area(m^2)	Sails high(m)	Chord length(m)	Aspect ratio	Sail thickness(m)
1	0.638	0.5	0.46	1.087	0.045
2	0.638	0.5	0.46	1.087	0.113
3	0.638	0.5	0.46	1.087	0.217

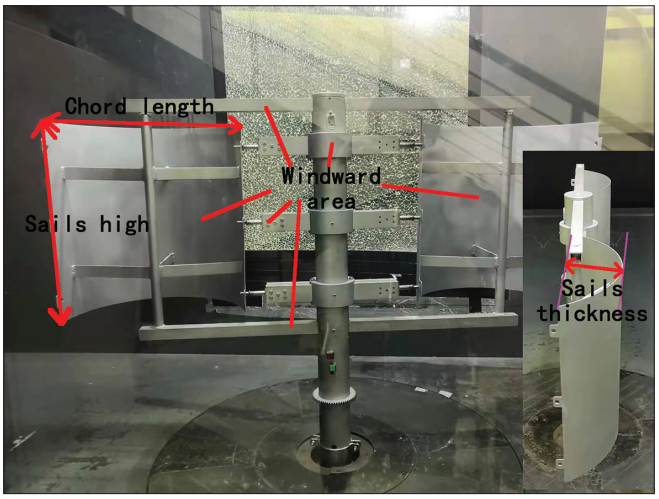

Fig. 3. Basic parameters identification of multi-mode sailing device

WIND ASSIST TEST

The force test of the wind sail model is carried out in a uniform flow field. The zero position of the turntable corresponds to the zero position of the dynamometer and coincides with the wind tunnel coordinates. The model was mounted at the 0° angle of attack position. After the model was installed, data acquisition and zero calibration were performed in the windless state, then the fan was started. After the test wind speed was reached and stabilized, the data were measured and recorded. The turntable was rotated from the 0° angle of attack counterclockwise at 5° intervals to measure the forces at different angles of attack.

The aerodynamic force of the sail is decomposed into two components, the lift force F_L perpendicular to the incoming flow and the drag force F_d acting in line with the local wind direction, as shown in Fig. 4 [7, 8]. The wind direction angle θ is the angle between the wind speed vector and the sailplane direction, called the angle of attack of the sail. Since the wind direction does not change in the wind tunnel, the sail model can only rotate at different angles under the action of the turntable. The force of the sail model measured by the balance is based on the balance coordinates. The balance and the sail model follow the turntable together with the rotation angle θ. The measurement is performed on the balance. The lift force measured on the balance is F_Z and the drag force is F_X. When calculating the aerodynamic force of the sail at different angles of attack, the drag force F_d parallel to the wind speed direction and the lift

force F_L perpendicular to the wind speed direction, need to be obtained by coordinate transformation, and then the lift force coefficient C_L and drag force coefficient C_d at different angles of attack are calculated according to the model and test parameters.

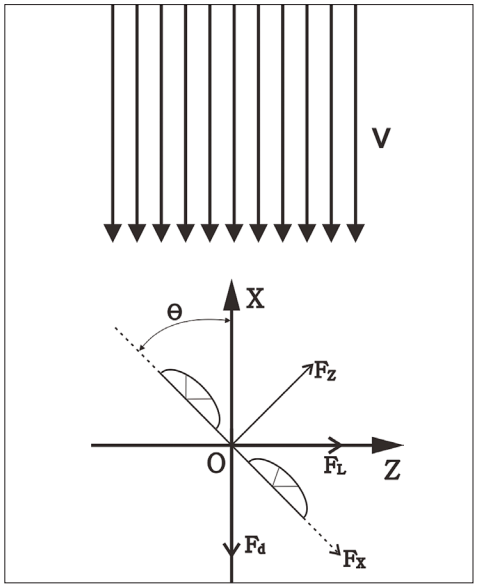

Fig. 4. The force diagram of multi-mode sail device

The lift force of the sail is [9, 10, 11]

$$F_L = F_Z\cos\theta + F_X\sin\theta \tag{1}$$

The drag force F_d is

$$F_d = F_X\cos\theta - F_Z\sin\theta \tag{2}$$

The lift force coefficient and drag force coefficient are expressed as

$$C_L = 2F_L/\rho V^2 S \tag{3}$$

$$C_d = 2F_d/\rho V^2 S \tag{4}$$

In Eq. (3) and Eq. (4), S is the windward area of the sail and ρ is the air density. According to the temperature and air pressure measured during the test, the air density is 1.26 kg/m^3 and V is the test wind speed.

During the test, when air flows through the test device, the device has an obstructive effect on the cross-section of the airflow channel. As the angle of attack changes, the cross-sectional area of the device changes in the direction of the airflow, and the obstruction changes accordingly. The walls of the wind tunnel restrict the airflow from expanding and spreading outward, allowing the airflow through the device to accelerate through the test device.

According to the law of continuity, the relationship between the test wind speed and the corrected wind speed can be derived.

$$\rho A_1 V_1 = \rho A V \tag{5}$$

When the wind speed is below Mach 0.3, the air density ρ can be regarded as incompressible fluid flow and the density remains constant. A_1 is the cross-sectional area of the wind tunnel test section, located at the front of the test section, V_1 is the air velocity entering the test section, set by the experiment, A is the cross-sectional area of the airflow at the location of the test device, and V is the corrected velocity of the airflow when flowing through the device.

From the formula (5), we get:

$$V = A_1 V_1 / A \tag{6}$$

The forces on the sails for different angles of attack and thickness at test wind speeds of 5 m/s, 10 m/s, and 15 m/s are shown in Fig. 5, Fig. 6, and Fig. 7.

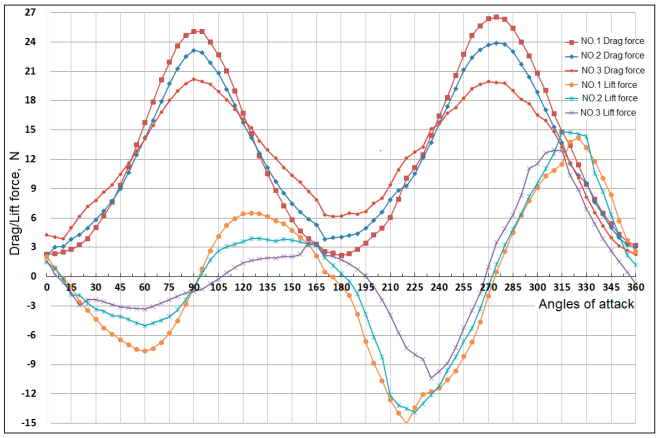

Fig. 5. Curves of sail lift forces and drag forces under different thickness at 5 m/s wind speed

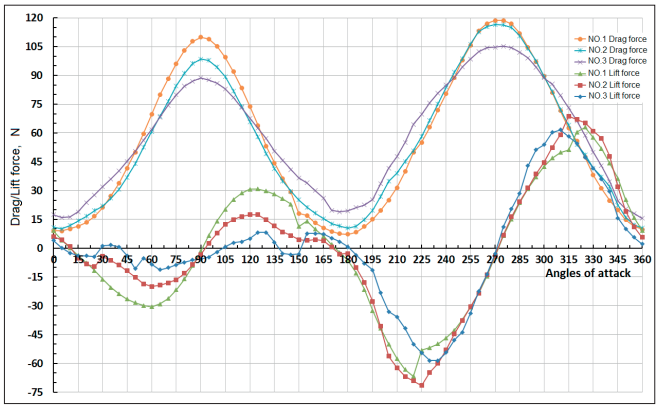

Fig. 6. Curves of sail lift forces and drag forces under different thickness at 10 m/s wind speed

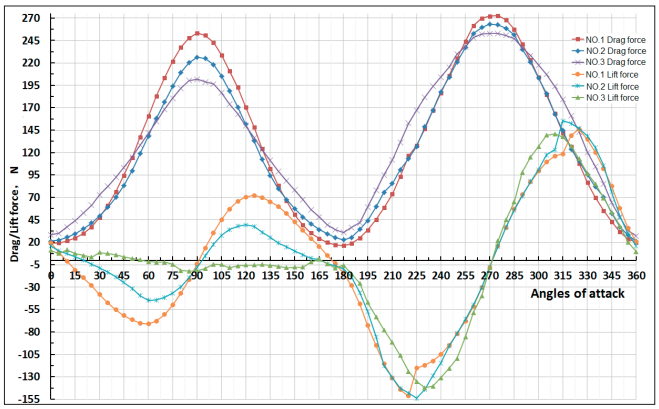

Fig. 7. Curves of sail lift forces and drag forces under different thickness at 15 m/s wind speed

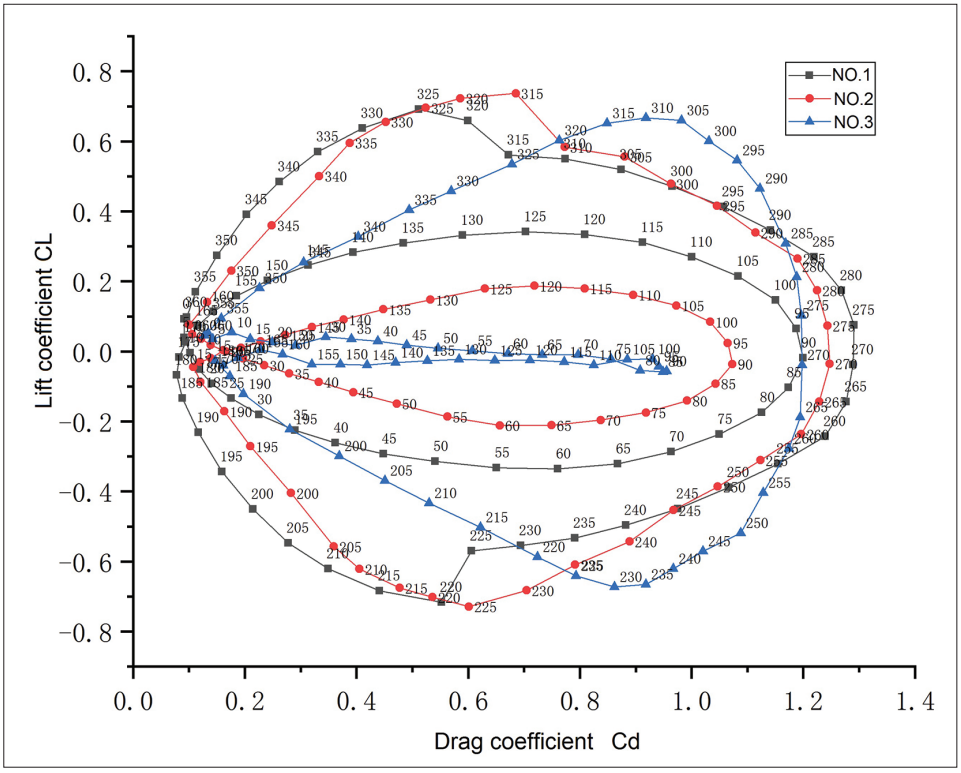

Fig. 8. Curves of lift coefficients and drag coefficients of sails with different thickness

The C_L – C_d curves for the different thicknesses of the sail at the same wind speed are shown in Fig. 8.

From Figs. 5 to 7, it can be seen that the shapes of the corresponding lift-drag curves are approximately the same for different wind speeds, which indicates that the aerodynamic characteristics are not related to the wind speed, but the shape of the sail under the test conditions. During the rotation of the sail, when the concave and convex sides are perpendicular to the wind direction, the area exposed to the wind is the largest, and the drag force has two peaks. At this point, the lift force is almost zero. The angle between the device and the incoming flow is symmetrical, giving the same symmetrical flow field. The resistance curve is symmetrical to the incoming flow, showing the overall force symmetry. The lift force curves are symmetrical at 90° and 270° angles of attack, creating point symmetric curves of equal magnitude and opposite direction. The lift and drag coefficients for the three sails at different angles of attack are shown in Fig. 8. It should be noted that they have good symmetry in the upper and lower halves.

There are negative lift force values in Figs. 5 to 7, corresponding to the negative lift coefficient in Fig. 8. This is due to the measured values following the rotation of the balance, which is in the opposite direction of the fixed setup positive lift force. After the sail angle is greater than 180°, the upwind lift resistance of the concave surface is greater than that of the convex surface. When the angle of attack is between 210°–240° and 300°–330°, when the angle between the concave surface and the airflow is between 30° and 60°, the device has the maximum lift force. At this time, the maximum lift force is near the 45° airflow angle. When the device is perpendicular to the direction of the airflow, the wind resistance of the concave surface is the largest.

SAILING AID AND ENERGY SAVING APPLICATION

A ship needs to maintain a certain heading (x-axis direction) when sailing. As shown in the wind axis coordinate system in Fig. 9, the ship's navigation is influenced by the apparent wind speed V_b, which is generated by the combination of the wind speed V_z and the sailing speed V_c. On the route, the wind direction and wind speed are constantly changing with time. The sail-assisted ship must operate the sail and change the windward angle of the sails so that the ship gets the maximum thrust in the forward direction [10]. That angle of attack that produces the most boosting force on the ship and has the least effect on the stability of the ship is an important factor in measuring the performance of the sail.

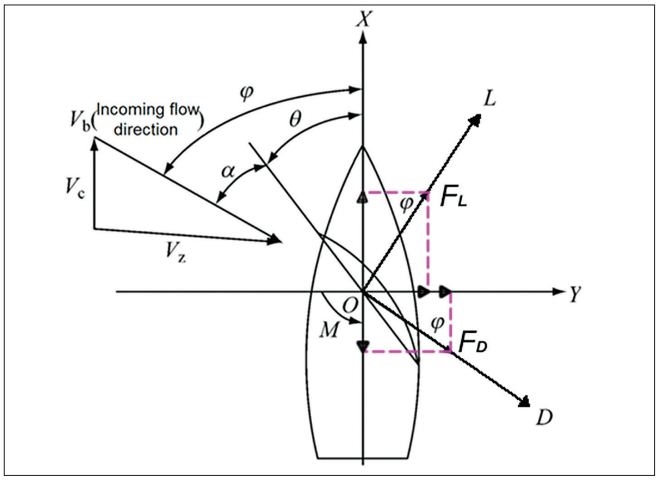

Fig. 9. The force analysis diagram of the sail on the ship

Fig. 9 shows the rectangular coordinate system O–LDZ [12], with the origin O at the center of the model bottom plate, the Z-axis vertically upright, the L-axis on the horizontal plane in the direction of lift, and the D-axis in the direction of drag. The aerodynamic force on the sail is decomposed into a drag force F_D along the incoming direction, a lift force F_L perpendicular to the incoming direction, and a torque M on the mast, with the reference point of the moment being the origin O.

According to the force analysis in Fig. 8, the boosting force produced by the sail on the boat is [13]:

$$T = F_L \sin\varphi - F_D \cos\varphi \tag{7}$$

The lateral force generated by the sail on the ship is:

$$H = F_L \cos\varphi - F_D \sin\varphi \tag{8}$$

Transformation of Eq. (7) yields:

$$T = \left(\frac{F_L}{\sqrt{F_L^2 + F_D^2}} \sin\varphi - \frac{F_D}{\sqrt{F_L^2 + F_D^2}} \cos\varphi\right)\sqrt{F_L^2 + F_D^2}$$
$$= A\left(\cos\beta \sin\varphi - \sin\beta \cos\varphi\right) = A\sin(\varphi - \beta) \tag{9}$$

Making the same transformation for Eq. (8), we get:

$$H = \left(\frac{F_L}{\sqrt{F_L^2 + F_D^2}} \cos\varphi + \frac{F_D}{\sqrt{F_L^2 + F_D^2}} \sin\varphi\right)\sqrt{F_L^2 + F_D^2}$$
$$= A\left(\cos\beta \cos\varphi + \sin\beta \sin\varphi\right) = A\cos(\varphi - \beta) \tag{10}$$

where $A = \sqrt{F_L^2 + F_D^2}$ called the modulus of lift force, and drag force being $\tan\beta = F_D/F_L$.

To make the maximum boosting force on the ship, there must be $\sin(\varphi - \beta) = 1$. At this time, the sail on the ship produces the maximum boosting force for A, the wind angle φ ranges from 0°–180°, β for 0°–90°, and $\varphi - \beta = 90°$, so that there is maximum boosting force and minimum lateral force.

According to the formula of A, the lift and drag forces obtained by the three sets of sails at different angles of attack are calculated and then the maximum value of A is selected. Maximum boosting forces are shown in Table 2.

Tab. 2. Maximum boosting force Unit: N

Wind Speed	No.1	No.2	No.3
5 m/s	26.53	24	20.87
10 m/s	118.87	116.56	107.96
15 m/s	273.11	263.49	256.51

Fig. 10 shows the maximum boosting force curves of the three arc sails at different wind speeds.

It can be seen that when the thickness is minimum, the boosting force is maximum, and the larger the thickness, the smaller the maximum boosting force. The curves of No. 1 and No. 2 are closer, but there is not much difference in the values of the three.

The lift force and drag force data from wind tunnel tests of the device at different wind speeds were substituted into Eq. (7) and (8) using different wind angles φ between 0° to 180°, and different angles of attack in turn at the selected wind angles. To calculate the boosting force and lateral force of the ship, selecting the maximum boosting force obtained at all angles of attack at a fixed wind direction and the corresponding lateral force to form the maximum boosting force and lateral force curves of the three sets of sails is shown in Fig. 11.

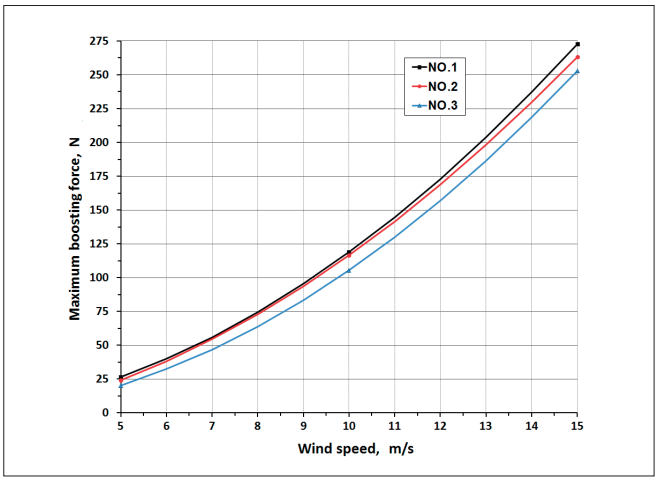

Fig. 10. Curves of maximum boosting force of sails under different wind speeds

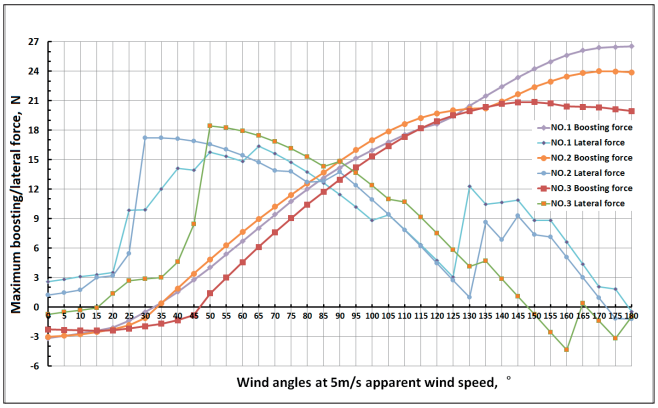

Fig. 11. Curves of maximum boosting force and corresponding lateral force of three sets of sails under different wind angles at 5 m/s apparent wind speed

Fig. 11 shows that for the sail with the largest thickness, the boosting force is negative when the wind angle is less than 50°, regardless of how the angle of attack is adjusted. For the other two sails, the boosting force is negative when the wind direction angle is less than 35°. As the wind direction angle increases, it is possible to obtain a gradually increasing boosting force by turning the sail angle of attack. When the wind angle is greater than 50°, the lateral force of the three sets of sails starts to decrease as the wind angle increases.

Fig. 11 shows that in the range of $35° < \varphi < 125°$, the boosting force of the three sets of sails increases with the increase of the wind direction angle, while the lateral force gradually decreases overall, with the smallest lateral force near 125°.

Generally, the speed of most ships is in the range of 10–30 knots, wind speed is in the range of 0–5 knots, and the sailing speed of ships is greater than wind speed in most cases. When the angle between wind speed and heading speed is small,

although the apparent wind speed obtained becomes larger, the angle between apparent wind speed and the heading is smaller, and it is difficult for the sail to produce an effective boost at a small angle. On the contrary, when the angle between wind speed and the heading speed is larger, it can make the angle between the apparent wind speed and course become larger and in the range of positive boost, but the apparent wind speed will become smaller and the boosting force to the boat will become smaller [14].

This device is suitable for ships sailing at low speeds around 10 knots. In most cases, the wind speed is not much different from the ship's speed, or the wind speed is greater than the ship's speed. Thus, the apparent wind speed can be kept at a large value and within the range of the positive boost angle in a wide range. According to Fig. 11, the apparent wind speed size and the angle formed by traversing the ship's speed, the possible wind speed angle change can be calculated. The apparent wind speed is in the range of less than 120° wind angle in most cases, in which the boosting force of sail No. 2 is greater than sail No. 1 and No. 3. When the wind speed is greater than the ship's speed, and the angle between the wind speed and the sailing speed is greater than 120°, then it is possible to enter the wind direction angle greater than 120°. At this time, the boosting force of sail No. 1 is greater than sails No. 2 and No. 3.

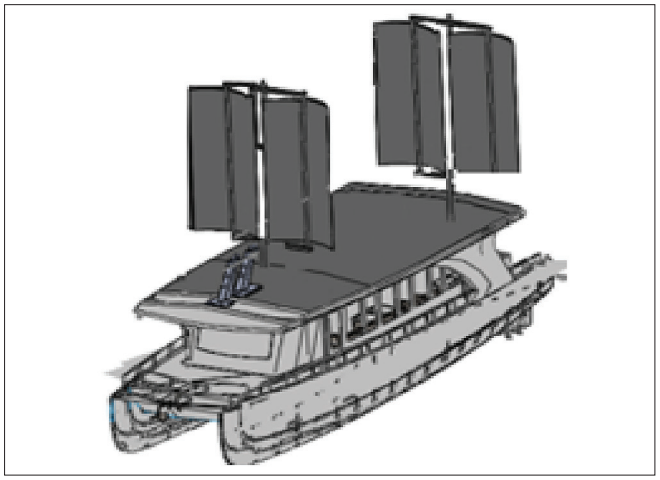

Fig. 12. Schematic diagram of installation of sailing yacht

The sail test results show that the sail blade with the smallest thickness has a better boosting effect in most working conditions. The wind speed is greater than the ship's speed when the apparent wind speed of the first sail is 5 m/s, with the wind direction angle of 120°, the boosting force is larger and the lateral force is smaller, and the maximum boosting force can reach 19.7 N. If two sets of sail devices are made according to the actual size with a similarity ratio of 10, considering the mutual influence of the sail arrays [15], the two devices can be staggered and installed on a yacht, as shown in Fig. 12. This can be applied only when the relative wind direction is exactly along the middle connecting direction, with the fore and aft sails of the device array being affected. According to the literature [15], the interference effect between the two sails becomes weaker when the distance between the two sails is greater than 2 times the chord length and is not considered in this estimation. When the wind direction angle of sail No. 1 is 120° and the apparent wind speed is 5.0 m/s, it will generate a boosting force of 3940 N, which is 19.7 kW. A 20 m long, 4.5 m wide excursion boat with a design speed of 13 knots and a rated power of 194 kW [16], the sail can be boosted up to 10.15% of the rated power. With the sail booster, the relationship between the power P_r consumed by the ship, the propeller output power P_P, the main engine output power P_e, and the sail booster power P_S when the yacht maintains a constant speed can be expressed as:

$$P_r = P_P \eta_P + P_S \eta_S = P_e \eta_C \eta_P + P_S \eta_S \tag{11}$$

Where, η_P is the overall efficiency of the propeller, η_C is the comprehensive efficiency of the main engine drive system, η_S is the comprehensive efficiency of the sailing aid system [17].

From Eq. (11), it can be seen that P_r remains unchanged when sailing at a constant speed, the power applied to the hull by the sail is the reduced power of the main engine. The main engine of the ship can run at reduced power (i.e. reduce the throttle opening of the main engine and the fuel consumption of the main engine will be reduced). If the diesel engine propulsion power η_1 is of the rated power of the main engine, after using the sail, the power of the main engine drops to η_2 approximately, and the fuel-saving per hour is:

$$\Delta G = P_e g_1 \eta_1 - P_e g_2 \eta_2 \tag{12}$$

Where g_1 represents the fuel consumption of the main engine, and g_2 indicates the fuel consumption after the addition of sails.

In the R. Hongying [17], on an 80,000 ton bulk carrier with propulsion power of 8833 kW, it is calculated that when the sail device provides a 12% boosting force, the main engine fuel consumption rate g_1 is reduced from 168.47 g/(kW·h) to g_2 165.58 g/(kW·h). Calculated on 200 sailing days per year, the fuel-saving is 806 t, and the fuel-saving per hour is 168 kg. It can be seen that after the main engine is running at reduced power, fuel consumption can be greatly reduced when its load level is reduced, the operating condition of components improve, service life of the diesel engine is extended, maintenance interval is extended, and the maintenance cost is reduced, thereby saving operating costs and achieving the goal of energy-saving and emission reduction.

WIND POWER GENERATION TEST

One side of the sail blade of the multi-mode sail device is rotated 180° to become a drag type wind turbine, as in Fig. 13, due to the asymmetric shape of the blade in the windward direction, causing a difference in air resistance. When there is a concave surface subject to resistance, F_1 is greater than the convex surface subject to resistance F_2. Therefore, the torque around the center axis is generated to rotate the wind wheel.

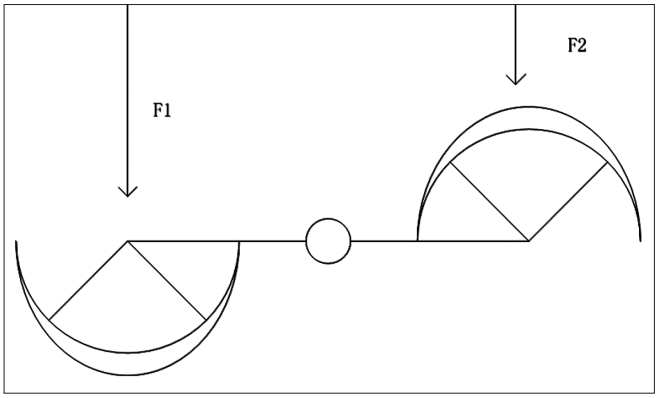

Fig. 13. Forces acting on sail blades in wind power generation mode

Wind tunnel tests were conducted in wind power generation mode to obtain the wind turbine speed and the output voltage of the disk motor at different wind speeds. Generally, in the wind power generation mode, the ship is in the suspended state. Compared to the wind boost mode, it lacks the self-navigation speed component when the apparent wind speed is relatively small. We selected the wind speeds of 4 m/s, 6 m/s, and 10 m/s for a wind power generation test. The disk generator used in the test has a rated speed of 36 r/min, a rated voltage of 13 V, and a rated power of 500 W. The test results are shown in Fig. 14 and Table 3.

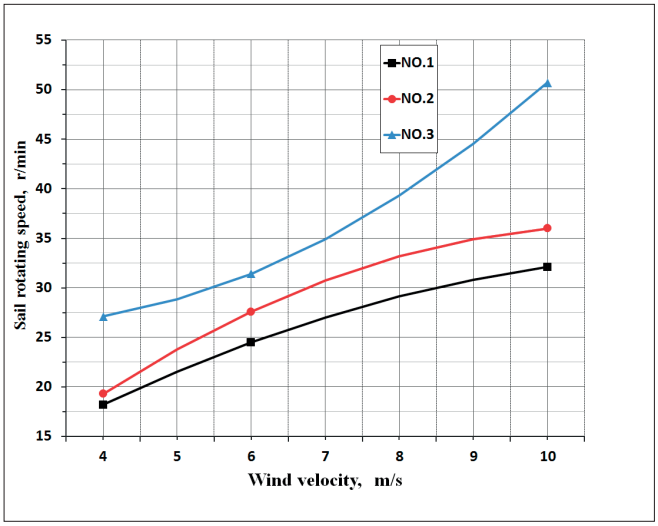

Fig. 14. Variation curve of wind turbine speed at different wind speeds

It can be seen in Fig. 14, that the slope of the speed curve of the No. 1 and No. 2 wind turbines gradually leans to be horizontal, indicating that the speed of the wind turbine will not increase indefinitely with the increase of wind speed. It shows that the operation state has been fully developed, and is not necessary to further increase the test wind speed, which also shows the rationality of the test wind speed we selected. The smaller the arc, the smaller the difference in air resistance between the concave surface and the convex surface. As the wind speed increases, the wind turbine speed increases. The concave surface runs in the direction of the incoming wind speed, resulting in a decrease in the relative wind speed. The convex surface runs in the opposite direction to the incoming wind speed, the relative wind speed increases, and finally the wind turbine stabilizes at a certain speed. Due to the fact that No. 3 has the largest thickness, the concave-convex surface is still in the stage where the speed increases with the wind under the test wind speed.

According to the data obtained from the wind tunnel test, within a certain range, the higher the wind speed, the greater the wind turbine speed, the greater the generating voltage. At the same wind speed, the greater the thickness, the greater the wind turbine speed. Large arcs will produce relatively small resistance when the convex surface is upwind, while the concave surface will produce relatively large resistance when it is downwind, and the total torque will be large. In the test, due to the uneven force of the blades in the forward and backward winds, the periodic lateral wind force occurred within a fixed angle range, which caused the sail device to generate periodic unbalanced forces and moments, causing the base of the device to withstand lateral forces and overturning moments. In the case of insufficient stiffness, violent shaking will occur especially when passing through the speed resonance zone.

CONCLUSIONS

The wind turbine blade turning and locking mechanism can switch between different operation modes of the multi-mode windsurfing device. Wind tunnel tests show that sail blades with small thickness have better-boosting effects, but low power generation efficiency. Sail blades with large thickness have good power generation effects but have lower boost efficiency and will produce larger lateral forces and overturning moments. No. 1 and No. 2 boost forces are not much different, but both are better than No. 3. However, in terms of power generation, No. 2 and No. 3 are the best, and No. 3 produces a larger lateral and overturning force under the same support rigidity condition. The requirements for the support of the sail and the structural strength of the device base are relatively high because the device needs to maintain certain rigidity and the connection of the base must be checked for fatigue strength. In the case of comprehensive consideration of the two modes of power generation and boosting, considering both boosting and power generation, the No. 2 sail is the best choice.

Tab. 3. Wind power test results

	RPM (r/min)			Output Voltage (V)		
Wind Speed	No. 1	No. 2	No. 3	No. 1	No. 2	No. 3
4 m/s	18.2	19.3	27.1	11.35	11.6	12.24
6 m/s	24.5	27.6	31.43	12.62	12.89	13.31
10 m/s	32.1	36	50.7	13.39	13.56	15.12

The lateral force on the sail causes the ship to drift angle, and to maintain the course, the rudder must be steered to overcome the lateral force. Thus, the additional drag force caused by the rudder to balance the lateral force must be considered. In the power generation mode, the rotation of the device generates unbalanced lateral forces and moments. It is necessary to further check the structural strength of the ship, avoid the speed resonance zone, and study the effect of the rotation on the additional lateral forces of the ship and the course stability.

ACKNOWLEDGMENTS

The authors wish to thank the Science & Technology Commission of Shanghai Municipality and Shanghai Engineering Research Center of Ship Intelligent Maintenance and Energy Efficiency (Grant No. 20DZ2252300).

REFERENCES

1. T. C. Van, J. Ramirez, T. Rainey, Z. Ristovski, R. J. Brown, "Global impacts of recent IMO regulations on marine fuel oil refining processes and ship emissions", *Transportation Research Part D: Transport and Environment*, vol. 70, pp. 123–134, 2019. doi: 10.1016/j.trd.2019.04.001.

2. T. Chou, V. Kosmas, M. Acciaro, K. Renken, "A comeback of wind power in shipping: An economic and operational review on the wind-assisted ship propulsion technology", *Sustainability*, vol. 13, pp. 1880, 2021. doi: 10.3390/su13041880.

3. Y. Ling, X. Cai, "Exploitation and utilization of the wind power and its perspective in China", *Renewable and Sustainable Energy Reviews*, vol. 16, pp. 2111–2117, 2012. doi: 10.1016/j.rser.2012.01.039.

4. O. Ellabban, H. Abu-Rub, F. Blaabjerg, "Renewable energy resources: Current status, future prospects and their enabling technology", *Renewable and Sustainable Energy Reviews*, vol. 39, pp. 748–764, 2014. doi:10.1016/j.rser.2014.07.113.

5. F. Yu, X. Li, F. Fan, S. Qiang, "Feasibility analysis of dual-purpose wind energy device on river-sea bulk carrier", *China Ship Repair*, vol. 30, pp. 17–20, 2017. doi: 10.13352/j.issn.1001- 8328.2017.03.006.

6. Z. Xiangming, H. Yihuai, W. Youcong, "Wind tunnel test on sails with different shape", *Journal of Shanghai Maritime University,* vol. 31, pp. 28–31, 2010.

7. F. Tillig, J. W. Ringsberg, "Design, operation and analysis of wind-assisted cargo ships", *Ocean Engineering*, vol. 211, pp. 107603, 2020. doi: 10.1016/j.oceaneng.2020.107603.

8. M. Pawłusik, R. Szłapczyński, A. Karczewski, "Optimising rig design for sailing yachts with evolutionary multi-objective algorithm", *Polish Maritime Research*, vol. 27, no. 4, 2020. doi: 10.2478/pomr-2020-0064.

9. D. Li, Y. Zhang, P. Li, J. Dai, G. Li, "Aerodynamic performance of a new double-flap wing sail", *Polish Maritime Research*, vol. 26, pp. 61–68, 2019. doi: 10.2478/pomr-2019-0067.

10. J. He, Y. Hu, J. J. Tang, S. Xue, "Research on sail aerodynamics performance and sail-assisted ship stability", *Journal of Wind Engineering and Industrial Aerodynamics*, vol. 146, pp. 81–89, 2015. doi: 10.1016/j.jweia.2015.08.005.

11. Y. Hu, X. Zeng, S. Li, "Research on the aerodynamic characteristics of ellipse wing sail". *Advanced Materials Research*, vol. 347–353, pp. 2249–2254, 2012. doi: 10.4028/www.scientific.net/AMR.347-353.2249.

12. Z. Xiangming, Z. Huawu, "Experimental study of the aerodynamics of sail in natural wind", *Polish Maritime Research*, vol. 25, pp. 17–22, 2018. doi: 10.2478/pomr-2018-0068.

13. D. E. Elger, M. Bentin, M. Vahs, "Comparison of different methods for predicting the drift angle and rudder resistance by wind propulsion systems on ships", *Ocean Engineering*, vol. 217, 108152, 2020. doi: 10.1016/j.oceaneng.2020.108152.

14. A. Babarit, G. Clodic, S. Delvoye, "Exploitation of the far-offshore wind energy resource by fleets of energy ships – Part 1: Energy ship design and performance", *Wind Energy Science*, vol. 5, pp. 839–853, 2020. doi: 10.5194/wes-5-839-2020.

15. Q. Li, Y. Nihei, T. Nakashima, Y. Ikeda, "A study on the performance of cascade hard sails and sail-equipped vessels", *Ocean Engineering*, vol. 98, pp. 23–31, 2015. doi: 10.1016/j.oceaneng.2015.02.005.

16. Yaguang Technology Group Co., "20m-FRP tour boat Performance" [Online]. (http://en.ygkjgroup.com.). Accessed on July 5,2021,

17. R. Hongying, H. Lianzhong, S. Peiting, L. Nan, "Comprehensive energy-saving and emission reduction potential of large sail-assisted ship", *Journal of Dalian Maritime University*, vol. 36, pp. 27–30, 2010. doi: 10.16411/j.cnki.issn1006-7736.2010.01.016.

CONTACT WITH THE AUTHORS

Huawu Zhang
e-mail: zhanghw@shmtu.edu.cn

Shanghai Maritime University
1550 Haigang Dadao,PuDong New Area
201306 Shanghai
China

Yihuai Hu
e-mail: yhhu@shmtu.edu.cn

Shanghai Maritime University
1550 Haigang Dadao,PuDong New Area
201306 Shanghai
China